Reactivity of Laser-Prepared Copper Nanoparticles: Oxidation of Thiols to Disulfides

Tung-Yu Chen,[†] Shin-Fu Chen,[†] Hwo-Shuenn Sheu,*[,‡] and Chen-Sheng Yeh*[,†]

Department of Chemistry, National Cheng Kung University, Tainan, Taiwan 701, ROC, and Synchrotron Radiation Research Center, Hsinchu 30077, Taiwan, ROC

Received: March 1, 2002; In Final Form: May 20, 2002

A series of alkanethiols, *n*-decanethiol ($C_{10}SH$), *n*-dodecanethiol ($C_{12}SH$), *n*-tetradecanethiol ($C_{14}SH$), *n*-hexadecanethiol ($C_{16}SH$), and *n*-octadecanethiol ($C_{18}SH$), were introduced to study the reactivity of the laser-prepared Cu nanoparticles. The colloidal solutions containing alkanethiols resulted in the disulfide (RSSR) formation. In particular, the colorless and the lathy crystals were generated from the $C_{14}SH$, $C_{16}SH$, and $C_{18}SH$. The psuedo-one-dimensional lathlike structures were resolved by the X-ray crystallographic analysis. UV−vis, TEM, high-resolution XRD, and proton NMR were carried out to characterize the Cu nanoparticles and the disulfide products. XPS and XANES measurements were employed to identify the Cu identity, as well. The laser-prepared Cu particles were mainly +0 charge with the possible formation of a thin Cu_2O layer on the copper surfaces. It was interpreted that the disulfides resulted from the Cu and/or Cu (core)/Cu_2O (thin shell) particles.

Introduction

Nanoscale materials have attracted significant scientific and industrial interest. The unique size-dependent properties of these nanocrystals have promising applications in catalysis, electronic and optical devices, and biological analysis.[1−4] Metallic Cu has shown the catalytic ability in the formation of aldehydes from the conversion of methanol and ethanol.[5,6] The micro-copper particles have been employed into a polyaniline film as the chemically modified electrodes for the detection of the amino acids and polyhydric molecules.[7] For the nano-Cu entities, colloidal preparations have been the essential aspect. Many techniques, such as chemical reduction,[8] radiolytic reduction,[9−11] and the reduction of copper ions using supercritical fluids,[12,13] were developed to synthesize spherical nanoparticles. In addition, different from the Cu particles, the morphology with the rod and fiber shapes have been reported.[14−16]

Recently, we demonstrated that the Cu nanoparticles could be formed without stabilizing agents using laser irradiation of CuO powders immersed in 2-propanol under aerobic conditions.[17,18] In this paper, a series of alkanethiols, *n*-decanethiol ($C_{10}SH$), *n*-dodecanethiol ($C_{12}SH$), *n*-tetradecanethiol ($C_{14}SH$), *n*-hexadecanethiol ($C_{16}SH$), and *n*-octadecanethiol ($C_{18}SH$), were oxidized as disulfides (RSSR) in the presence of Cu nanoparticles. In addition, different alkyl chain lengths resulted in distinct crystalline structures. $C_{14}SH$, $C_{16}SH$, and $C_{18}SH$ gave rise to the lathlike colorless crystals observed for the first time, while reddish-brown precipitates were produced from both $C_{10}SH$ and $C_{12}SH$. In previous studies the surface chemistry of the alkanethiols on the copper substrates, i.e., the powders, the polycrystalline sheets, and the thin films, showed the disulfide formation.[19,20] Thiols were oxidized as disulfides on the CuO surfaces. The oxide layers (CuO) were then reduced to form Cu_2O and/or Cu. Subsequently, the thiols bound to the reduced surfaces as the thiolate species.[19,20]

* To whom correspondence should be addressed. E-mail addresses: csyeh@mail.ncku.edu.tw; hsheu@srrc.gov.tw.
[†] National Cheng Kung University.
[‡] Synchrotron Radiation Research Center.

Experimental Section

The Cu nanoparticles were generated by laser irradiation of CuO powders (99.999%, 80−100 mesh) in 2-propanol. Pyrex vials were used as containers to prepare the colloidal solutions. An unfocused Nd:YAG laser (Quantel Brilliant) operated at 10 Hz (5 ns pulse width) with a wavelength of 1064 nm was conducted through the opening into the vials containing 0.02 g of CuO powders and 5 mL of 2-propanol. The Cu colloidal solutions were prepared as follows: a laser intensity of 100 mJ/pulse was employed to irradiate mixtures including CuO powders and 2-propanol for 5 min, followed by centrifugation to remove the remaining CuO powders. Subsequently, the prepared solutions were illuminated for an additional 5 min. The resulting Cu colloidal solutions appeared a deep wine-red color. Laser intensities up to 300 mJ/pulse could be used to prepare Cu colloids. The ablated solutions were routinely stirred every 2 min in the course of irradiation. All manipulations were carried out under aerobic conditions. Immediately after the colloidal preparations, 0.5 mL of the *n*-decanethiol (Fluka, ≥95%), *n*-dodecanethiol (Fluka, ≥97%), *n*-tetradecanethiol (Fluka, ≥98%), *n*-hexadecanethiol (Lancaster, 98%), and *n*-octadecanethiol (Aldrich, 98%) were added into Cu colloidal solutions with approximate 9×10^{-4} mol L^{-1},[21] respectively. Following Belloni et al. methodology,[11] the Cu colloidal concentrations were calculated on the basis of the $\epsilon_{\lambda=570nm} = 1950$ L mol^{-1} cm^{-3}. The solid *n*-octadecanethiol was warmed to 35 °C in liquid form for use.

The UV−vis extinction spectra of the colloidal suspensions within an optical cell (optical path = 1 cm) were recorded using a Hewlett-Packard Model 8453 UV−VIS spectrometer. SEM images were carried out with a Hitachi S4100 field emission scanning electron microscope. Proton NMR spectra were measured by means of a Bruker AVANCE 300 MHz spectrometer. The X-ray crystal structure was determined under a Bruker AXS Smart-1000 single-crystal diffractometer. X-ray powder diffraction data for the structure analysis were collected at the wiggler beamline BL17A of the Synchrotron Radiation Research Center (SRRC), Taiwan, using a triangular bent Si(111)

10.1021/jp0205822 CCC: $22.00
Published on Web 08/29/2002

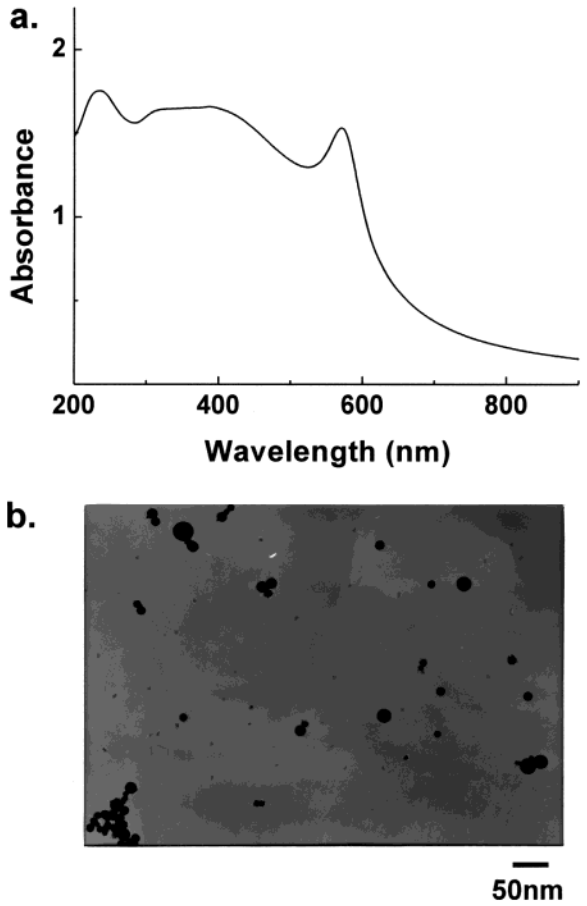

Figure 1. (a) Typical UV−vis absorption spectra of the Cu particles prepared in 2-propanol by 1064 nm laser light; (b) TEM image of the resulting Cu particles.

monochromator and a wavelength of 1.326 31 Å. The sample in a flat plate was mounted on the Huber 5020 diffractometer. The 2θ range is 0.3−90°. To improve the counting statistics at higher 2θ angles and the resolution at the angle below 10°, the pattern was divided into two regions, and the time per step for each region set accordingly. The data were then normalized using the monitor counts. The XPS was performed using a Fison (VG) ESCA 210 electron spectroscope for chemical analysis. X-ray absorption spectra were recorded at wiggler beamline BL17C at SRRC Taiwan using fluorescence modes (one ionization chamber and one Lytle detector) on the powder samples. The X-ray absorption measurements were done at Cu K-edge using the Si(111) double-crystal monochromator. The energy calibration was made according to the K-edge of the Cu-foil. The E_0 energies were taken from the first derivatives of the spectra. Electron micrograph analysis used a transmission electron microscope (Hitachi FE-2000). The average diameter and size distribution were calculated using SigmaScan Pro5.0 software for image analysis.

Results and Discussion

The prepared Cu colloidal solutions appeared a deep wine-red color with the plasmon band at 570 nm, as shown in Figure 1. The resulting spherical Cu particles exhibited a large distribution in size. The average diameter was 50.2 ± 30.1 nm calculated from the TEM images. These observations are consistent with our earlier investigations.[17,18] Immediately after particle preparations, the thiols ($C_{10}SH$, $C_{12}SH$, $C_{14}SH$, $C_{16}SH$, and $C_{18}SH$) were individually mixed into the colloidal solutions. Adding thiols did not induce the colloidal colors to change at once. However, the colloidal appearance turned brown and the sediments increased while the solutions were aged. Interestingly, the colorless crystalline with the needlelike shapes were observed by prolonged storage of solutions containing $C_{14}SH$, $C_{16}SH$, and $C_{18}SH$. Usually, the needlelike crystals appeared after solutions were aged for 1 day.

Figure 2 displays the SEM images of the crystallization products attained from Cu/$C_{16}SH$ solutions. As seen in these

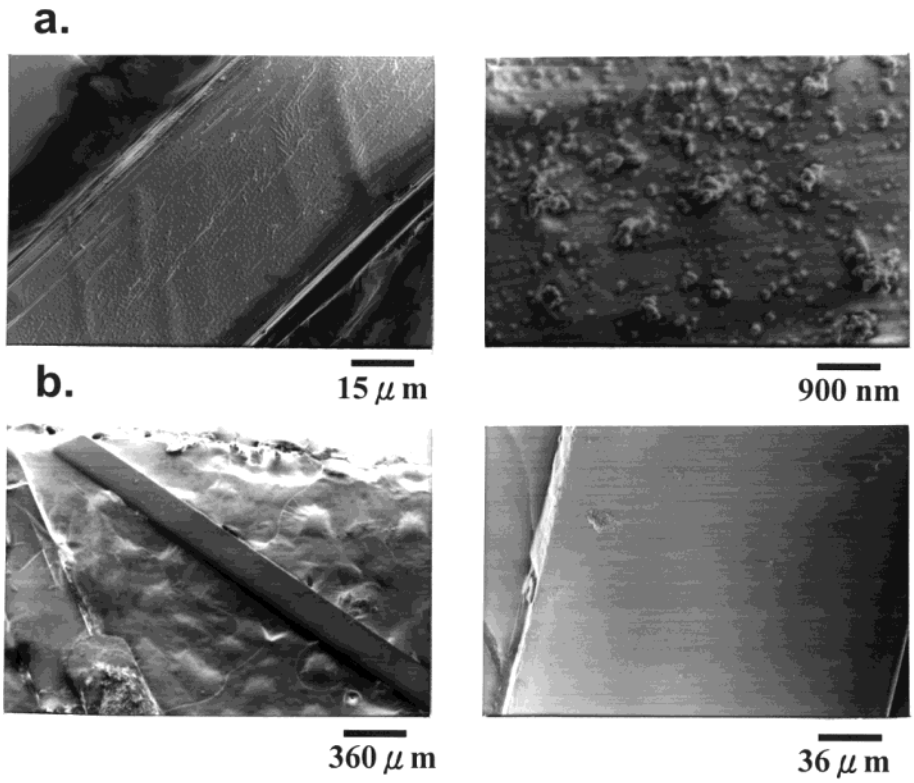

Figure 2. (a) SEM images of the lathy crystalline resulted from Cu/$C_{16}SH$ solutions; (b) the recrystallization products of the a crystals.

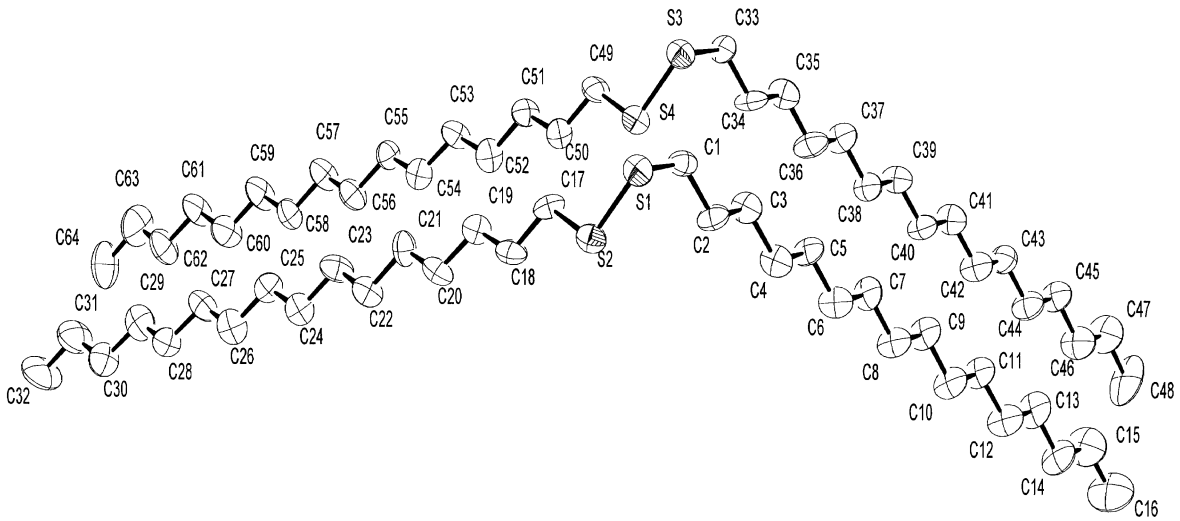

Figure 3. Crystal structure of the lathy crystalline. Selected bond lengths (Å) and angles (deg) (hydrogen atoms are omitted for clarity): S(1)−S(2), 2.029(6); S(3)−S(4), 2.030(6); S(1)−C(1), 1.792(17); S(3)−C(33), 1.833(15); S(2)−C(17), 1.825(16); C(1)−C(2), 1.54(2); C(17)−C(18), 1.521(19); C(1)−S(1)−S(2), 104.4(5); C(33)−S(3)−S(4), 103.9(5); C(17)−S(2)−S(1), 103.4(5); C(49)−S(4)−S(3), 102.0(5); S(1)−C(1)−C(2), 115.7(11); C(1)−C(2)−C(3), 111.8(14); S(2)−C(17)−C(18), 109.0(11); C(2)−C(3)−C(4), 113.0(14).

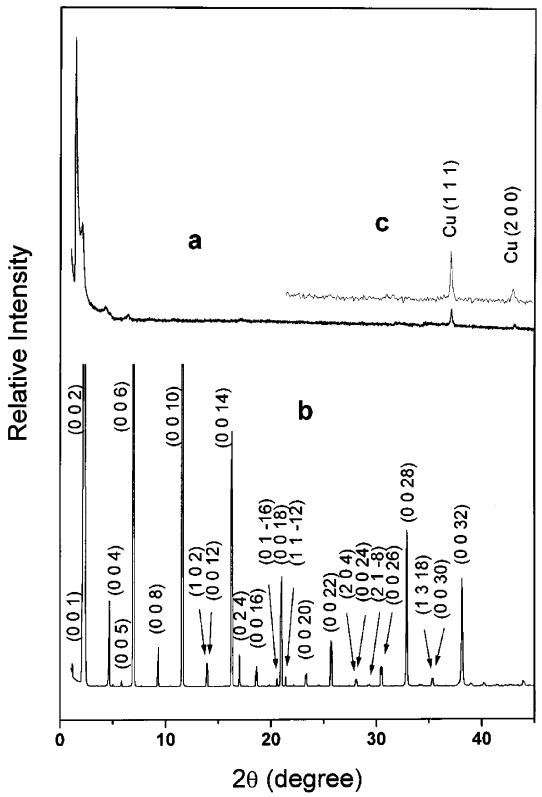

Figure 4. X-ray powder diffraction patterns of (a) the precipitates from the $Cu/C_{12}SH$ solutions, (b) the lathy crystals attained from $Cu/(C_{16}S)_2$ samples, and (c) the freshly prepared Cu nanoparticles. The indexing of b was based on the single crystal unit cell. The intensity scale of b was selected to enhance the smaller peaks in the patterns, allowing only a partial view of the most intense peaks.

images, the needle crystals are more like lathy structures. Their widths ranged from 7 to 300 μm, and the lengths could be up to millimeter scale. These crystalline species are fragile and are soluble to nonpolar solvents, such as cyclohexane and benzene. It was found that the copper particles randomly distributed on the surfaces of the crystals, as shown in Figure 2a. The particles could be separated out of these lathy structures via the recrystallization procedure. Recrystallization was performed by

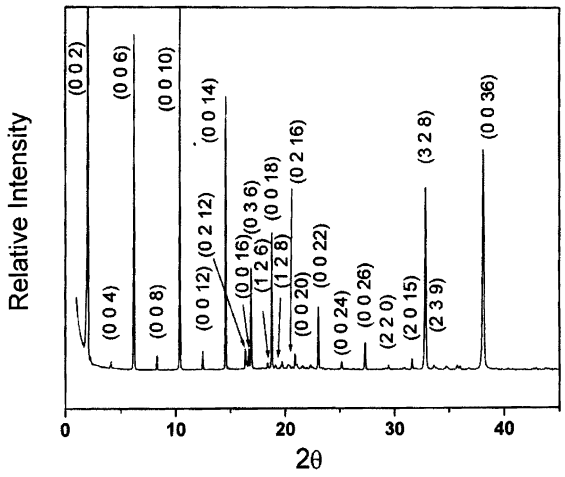

Figure 5. X-ray powder diffraction patterns of the lathy crystals attained from the $Cu/(C_{18}S)_2$ samples. The indexing was refined using the single crystal unit cell. The intensity scale was selected to enhance the smaller peaks in the patterns, allowing only a partial view of the most intense peaks.

warming the mixtures containing the lathy crystals and 2-propanol up to 50 °C, subsequently lowering the temperature under the controlled rate of 0.5 °C/h. Figure 2b reveals the recrystallization products. The X-ray crystallographic analysis of the recrystallization crystal showed that the disulfide structures (RSSR) constitute the crystalline lath, as shown in Figure 3 (Cambridge Crystallographic Data Center, CCDC 172104).[22] The crystal develops the preferred growing orientation. The parallel experiments were conducted by mixing $C_{14}SH$, $C_{16}SH$, or $C_{18}SH$ with the irradiated 2-propanol in the absence of Cu nanoparticles, as well. No such needlelike morphology could be seen, and solutions remained as thiols and 2-propanol components inspected by NMR. For the $Cu/C_{10}SH$ and $Cu/C_{12}SH$ solutions, the aggregation of copper particles resulted in the precipitates, but the NMR measurements verified the existence of the oxidation products, disulfides, in the solutions.

High-resolution XRD with synchrotron X-ray source (λ = 1.326 31 Å) was conducted to characterize the freshly prepared Cu particles, the precipitates from $Cu/C_{12}SH$ solutions, and the $Cu/(C_{16}S)_2$ and $Cu/(C_{18}S)_2$ lathy crystals. The XRD patterns of

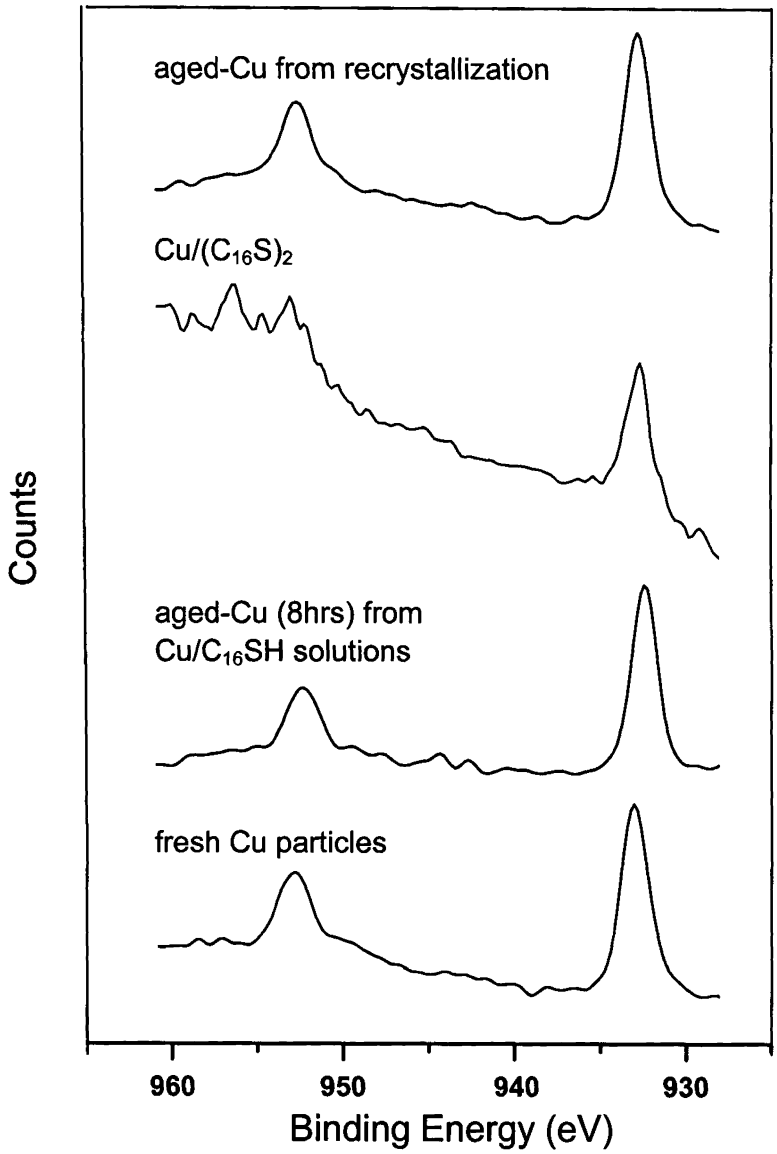

Figure 6. XPS spectra of the Cu2p region for the freshly prepared Cu particles, the Cu particles after aging $Cu/C_{16}SH$ for 8 h, the $Cu/(C_{16}S)_2$ crystals, and the aged-Cu particles collected from the recrystallization.

the freshly prepared Cu particles, the precipitates from Cu/C_{12}-SH solutions and the $Cu/(C_{16}S)_2$ are shown in Figure 4. All samples were in their original shapes without any grind for measurements. The samples of the $Cu/C_{12}SH$ solutions were in the form of reddish-brown powders. Figure 4a shows that the *d* spacings of the first four lines are 52.23, 36.88, 17.80, and 11.88 Å. The index by Treor failed to give a simple unit cell, but it is clear that one of the cell dimensions must be equal to or larger than 52 Å. For comparison, the XRD patterns of the corresponding freshly prepared Cu particles are shown in Figure 4c. The (1 1 1) and (2 0 0) reflections of the Cu clusters are located at 2.0842 and 1.8053 Å, respectively. As can be seen, the Cu diffraction peaks appeared in the $Cu/C_{12}SH$ XRD patterns. The XRD patterns of $Cu/(C_{16}S)_2$ are dramatically different from those of $Cu/C_{12}SH$ samples. Note that the lathy crystals containing Cu particles, as shown in Figure 2a, were used for XRD measurements. The unit cell of the $Cu/(C_{16}S)_2$ powder sample was refined on the basis of the single-crystal results as the initial values. The index of $Cu/(C_{16}S)_2$ is marked in Figure 4b. Most of the reflections are (0 0 1). The cell dimensions are $a = 5.57(5)$ Å, $b = 9.3(1)$ Å, $c = 65.59(6)$ Å, $\alpha = 88.6(16)°$, $\beta = 90.0(19)°$, $\gamma = 89.9(20)°$. The measured XRD pattern of $Cu/(C_{16}S)_2$ did not show the apparent Cu particle peaks. For the $Cu/(C_{18}S)_2$, the XRD patterns are very similar to those of $Cu/(C_{16}S)_2$. The refined cell dimensions of $Cu/(C_{18}S)_2$ are $a = 5.56(9)$ Å, $b = 14.57(4)$ Å, $c = 73.14(8)$ Å, $\alpha = 88.94$-$(19)°$, $\beta = 89.9(3)°$, $\gamma = 89.28(16)°$, as illustrated in Figure 5.

We have shown that the colloidal solutions with copper species resulted in thiol oxidation, leading to disulfide formation. In particular, the pseudo-one-dimensional lathy products were grown from $C_{14}SH$, $C_{16}SH$, and $C_{18}SH$. As mentioned earlier for the studies of the surface chemistry on the copper, the groups of Keller and Sung suggested that thiol oxidation accompanied with the disulfide formation by the reduction of the Cu^{2+} state as Cu^+ or Cu on the CuO surfaces and the alkanethiols adsorbed on the reduced surfaces (Cu and Cu_2O) as RSCu identities.[19,20] Our measurements of the freshly prepared Cu nanoparticles on XRD indicated no sign of the copper oxide species, as seen in Figure 4c. To further verify the particle properties, the XPS analysis was carried out. Figure 6 displays the typical XPS spectra of the Cu2p region for the freshly prepared Cu particles, the Cu particles from the aged $Cu/C_{16}SH$ solutions for 8 h before yielding lathy crystals, the $Cu/(C_{16}S)_2$ lathy crystals, and the aged-Cu particles collected from the recrystallization. It was

TABLE 1: XPS Binding Energies of Cu2p and S2p Peaks for The Copper-Containing Materials

	binding energy (eV)			
	Cu		S[a]	
sample	$2p_{3/2}$	$2p_{1/2}$	$2p_{3/2}$	$2p_{1/2}$
fresh Cu particles	932.9	952.7		
$Cu/(C_{16}S)_2$ crystals	932.6	953.1	163.2	164.4
$Cu/(C_{18}S)_2$ crystals	932.9	952.6	163.7	164.9
aged-Cu particles	932.7	952.5	161.9	163.2

[a] The $S2p_{3/2}$ and $S2p_{1/2}$ were determined by fitting the experimental spectra with a 2:1 area ratios and a 1.2 eV separation.

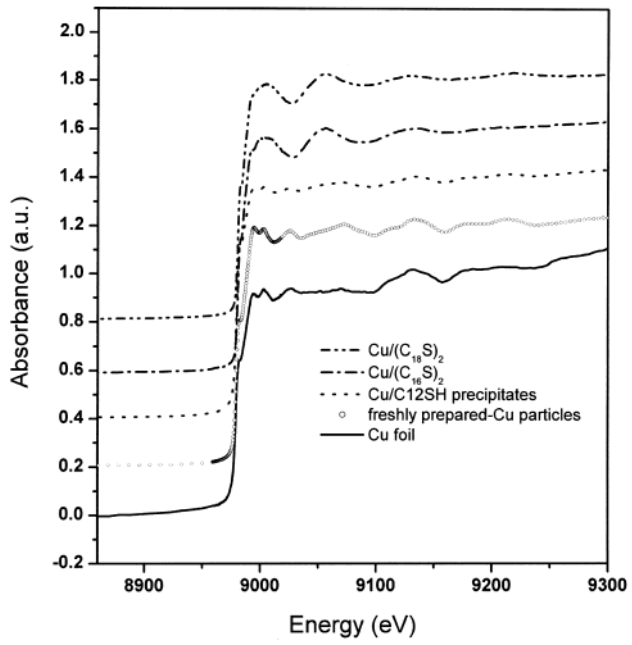

Figure 7. Cu K-edge XANES spectra of the Cu foil, the freshly prepared Cu particles, the precipitates from $Cu/C_{12}SH$ solutions, the $Cu/(C_{16}S)_2$, and the $Cu/(C_{18}S)_2$ crystals. The baseline of each compound is shifted in vertical for the purpose of the clarification.

found that no characteristic shake-up peaks corresponding to the Cu^{2+} state formation appeared between 940 and 945 eV.[20,23] The XPS detected the $Cu2p_{3/2}$ and $Cu2p_{1/2}$ at 932.9 and 952.7 eV, respectively, for the freshly prepared Cu particles, as seen in Table 1. The $Cu2p_{3/2}$ and $Cu2p_{1/2}$ binding energies were also determined for the lathy crystals of the $Cu/(C_{16}S)_2$ and $Cu/(C_{18}S)_2$. The aged-Cu particles attained from the recrystallization produced values corresponding to $Cu2p_{3/2}$ at 932.7 eV and $Cu2p_{1/2}$ at 952.5 eV. On the basis of the XPS results from Table 1, the determined copper binding energies could be assigned as metallic Cu; it, however, was known that metallic Cu and Cu^{1+} could not be readily clarified.[23,24] In fact, the very small O1s peaks were observed around 532−535 eV for all of the measured samples. The oxygen signals might result from the oxide layer formation.

In addition to the XPS measurements, X-ray absorption near-edge spectroscopy (XANES) was performed to gain insight into the electronic structures of the copper centers. XANES is a powerful tool to determine the chemical state and local symmetry of the choice metal. XANES experiments at Cu K-edge (Figure 7) were performed to precisely determine the oxidation states of the Cu in freshly prepared Cu particles, $Cu/C_{12}SH$ precipitates, $Cu/(C_{16}S)_2$, and $Cu/(C_{18}S)_2$. The results are used to compare with Cu foil, which is considered as zero charge. The E_0 values are 8978.7, 8979.2, 8979.9, 8980.3, and 8980.6 eV for Cu in the Cu foil, the freshly prepared Cu particles, the $Cu/C_{12}SH$ precipitates, the $Cu/(C_{16}S)_2$, and the $Cu/(C_{18}S)_2$ crystals, respectively. We observed a more than 1 eV high-energy shift of the E_0 and the absorption maximum, due to the increase of the oxidation state from pure +0 (Cu foil) to +1 ($Cu/(C_{16}S)_2$ and $Cu/(C_{18}S)_2$). The spectra of the Cu foil and the freshly prepared Cu particles are practically identical. The E_0 energies and the features of the spectra above the edge for both Cu foil and freshly prepared Cu particles show that the oxidation of Cu is mainly +0 charge. However, the 0.5 eV (E_0) difference between the Cu foil and the freshly prepared Cu particles might suggest the existence of the Cu^{1+} state for the freshly prepared Cu particles. It is possible that the freshly prepared Cu particles are in a form of Cu^0 accompanied with a thin Cu_2O layer. The spectra of the $Cu/(C_{16}S)_2$ and $Cu/(C_{18}S)_2$ are very similar, but quite different from that of the Cu foil. The oscillation of the spectra above the edge is due to the coordination bond lengths and numbers, and the local geometric symmetry. Qualitatively, the coordination environments of the Cu in both $Cu/(C_{16}SH)_2$ and $Cu/(C_{18}S)_2$ are the same. The E_0 and the maximum absorption energies indicate that the Cu species in those two compounds ($Cu/(C_{16}SH)_2$ and $Cu/(C_{18}S)_2$) are mainly +1 charge. Interestingly, the $Cu/C_{12}SH$ sediments feature is intermediate between those of Cu foil and $Cu/(C_{16}S)_2$, but more resembles the Cu foil. This suggests that the Cu/C_{12}-SH samples have the simultaneous presence of the Cu^0 and Cu^+ states. Unfortunately, we have no further explanation to be given for such observation at this stage. Finally, the XANES results confirmed the electron transfer leading to the formation of the $CuSC_nH_{2n+1}$ where $n = 12$, 16, and 18. That is the copper-thiolate bonds formation for the Cu surfaces. Although the $Cu/(C_{14}S)_2$ crystals were not investigated, their properties should be approximate to those observed for $Cu/(C_{16}SH)_2$ and $Cu/(C_{18}S)_2$. Same outcomes would be expected for the $Cu/C_{10}SH$ precipitates as compared with the $Cu/C_{12}SH$. The XPS analysis on the S2p binding energies from the aged-Cu particles provided the further evidence of the alkanethiolate structures, as seen in Table 1. The aged-Cu particles attained from the recrystallization of the disulfide lathy crystals exhibited S2p signals assigned to $S2p_{3/2}$ (161.9 eV) and $S2p_{1/2}$ (163.2 eV), which are attributed to the thiolate species.[20,25−28] Herein, one intriguing observation is that the determined S2p showed the BEs above 163 eV for both $Cu/(C_{16}S)_2$ and $Cu/(C_{18}S)_2$ samples. It is known that the BEs of the unbound disulfides are located 163−164 and ∼165 eV for the $S2p_{3/2}$ and $S2p_{1/2}$, respectively.[25,28]

In summary, on the basis of the XPS and XANES studies, our laser-prepared Cu particles are mainly +0 charge with the possibility of forming a thin Cu_2O layer on the surfaces. Therefore, the resulting disulfides were induced from the presence of the Cu^0 and/or Cu^+ species. The possible mechanisms are considered that formation of disulfides, $(SC_nH_{2n+1})_2$, accompanied with the oxidative addition resulting in copper−thiolate bonds for the clean Cu and Cu_2O_{shell} surfaces. Such consequences are different from the previous investigations on the copper surfaces, where the disulfides formation took place on the CuO mantles and the alkanethiols bound to Cu_2O and Cu substrates. However, the detailed structures of the resulting precipitates from both $Cu/C_{10}SH$ and $Cu/C_{12}SH$ solutions remained to be resolved.

Acknowledgment. We thank the National Science Council of the Republic of China for financially supporting this work. We also acknowledge Ms. H. J. Shih for the SEM images, Mr. R. C. Lee for the XPS determination, and Ms. S. Y. Hsu and Mr. S. Y. Yao for the TEM and EDX measurements at Tainan Regional Instrument Center, National Cheng Kung University

and Ms. B. T. Ko for the X-ray analysis at Taichung Regional Instrument Center, National Chung Hsing University, ROC.

References and Notes

(1) Henglein, A. *J. Phys. Chem.* **1980**, *84*, 3461.
(2) Majetich, A.; Artman, J. O.; McHenry, M. E.; Nuhfer, N. T.; Staley, S. W. *Phys. Rev. B* **1993**, *48*, 16845.
(3) Storhoff, J. J.; Elghanian, R.; Mucic, R. C.; Mirkin, C. A.; Lestinger, R. L. *J. Am. Chem. Soc.* **1926**, *48*, 16845.
(4) Li, Y.; Hong, X. M.; Collard, D. M.; El-Sayed, M. A. *Org. Lett.* **2000**, *2*, 2385.
(5) Bowker, M.; Madix, R. J. *Surf. Sci.* **1980**, *95*, 190.
(6) Bowker, M.; Madix, R. J. *Surf. Sci.* **1982**, *116*, 549.
(7) Casella, I. G.; Cataldi, T. R. I.; Guerrieri, A.; Desimoni, E. *Anal. Chim. Acta* **1996**, *335*, 217.
(8) Huang, H. H.; Yan, F. Q.; Kek, Y. M.; Chew, C. H.; Xu, G. Q.; Ji, W.; Oh, P. S.; Tang, S. H. *Langmuir* **1997**, *13*, 172.
(9) Henglein, A. *J. Phys. Chem. B* **2000**, *104*, 1206.
(10) Delcourt, M. O.; Belloni, J. *Radiochem. Radioanal. Lett.* **1973**, *13*, 329.
(11) Khatouri, J.; Mostafavi, M.; Amblard, J.; Belloni, J. *Chem. Phys. Lett.* **1992**, *191*, 351.
(12) Cason, J. P.; Roberts, C. B. *J. Phys. Chen. B* **2000**, *104*, 1217.
(13) Ziegler, K. J.; Doty, C.; Johnston, K. P.; Korgel, B. A. *J. Am. Chem. Soc.* **2001**, *123*, 7797.
(14) Pileni, M. P.; Gulik-Krzywicki, T.; Tanori, J.; Filankembo, A.; Dedieu, J. C. *Langmuir* **1998**, *14*, 7359.
(15) Chen, P.; Wu, X.; Lin, J.; Tan, K. L. *J. Phys. Chem. B* **1999**, *103*, 4559.
(16) Salkar, R. A.; Jeeranandam, P.; Kataby, G.; Aruna, S. T.; Koltypin, Y.; Palchik, O.; Gendanken, A. *J. Phys. Chem. B* **2000**, *104*, 893.
(17) Yeh, Y. H.; Yeh, M. S.; Lee, Y. P.; Yeh, C. S. *Chem. Lett.* **1998**, 1183.
(18) Yeh, M. S.; Yang, Y. S.; Lee, Y. P.; Lee, H. F.; Yeh, Y. H.; Yeh, C. S. *J. Phys. Chem. B* **1999**, *103*, 799.
(19) Keller, H.; Simak, P.; Schrepp, W. *Thin Solid Films* **1994**, *244*, 799.
(20) Sung, M. M.; Sung, K.; Kim, C. G.; Lee, S. S.; Kim, Y. *J. Phys. Chem. B* **2000**, *104*, 2273.
(21) We gratefully acknowledge a reviewer's suggestion for evaluating Cu colloidal concentrations.
(22) Crystal data: $C_{64}H_{132}S_4$, $M = 1029.94$, triclinic, space group $P\bar{1}$, $a = 5.5639(8)$ Å, $b = 9.2765(13)$ Å, $c = 65.625(10)$ Å, $\alpha = 88.696(3)°$, $\beta = 89.774(3)°$, $\gamma = 89.055(3)°$, $V = 3385.8(9)$ Å^3, $T = 293(2)$ K, $Z = 2$, $\mu = 0.174$ mm^{-1}, $D_c = 1.010$ mg m^{-3}, 17 908 reflections measured, 11 842 independent reflections ($R_{int} = 0.0712$), which were used in all calculations. The final R1 = 0.1485 [$I > 2\sigma(I)$] for 11 842 data.
(23) Laibinis, P. E.; Whitesides, G. M. *J. Am. Chem. Soc.* **1992**, *114*, 9022.
(24) Ron, H.; Cohen, H.; Matlis, S.; Rappaport, M.; Rubinstein, I. *J. Phys. Chem. B* **1998**, *102*, 9861.
(25) Castner, D. G. *Langmuir* **1996**, *12*, 5083.
(26) Kang, S. Y.; Kim, K. *Langmuir* **1998**, *14*, 226.
(27) Han, S. W.; Kim, Y.; Kim, K. *J. Colloid Interface Sci.* **1998**, *208*, 272.
(28) Porter, L. A.; Ji, D.; westcott, S. L.; Graupe, M.; Czernuszewicz, R. S.; Halas, N. J.; Lee, T. R. *Langmuir* **1998**, *14*, 7378.